Measurements of atmospheric layers from the NASA DC-8 and P-3B aircraft during PEM-Tropics A

P. Stoller,[1] J. Y. N. Cho,[1] R. E. Newell,[1] V. Thouret,[1,2] Y. Zhu,[1] M. A. Carroll,[3] G. M. Albercook,[3] B. E. Anderson,[4] J. D. W. Barrick,[4] E. V. Browell,[4] G. L. Gregory,[4] G. W. Sachse,[4] S. Vay,[4] J. D. Bradshaw,[5,6] and S. Sandholm[5]

Abstract. Tropospheric vertical structure was analyzed using in situ measurements of O_3, CO, CH_4, and H_2O taken on board the NASA DC-8 aircraft during three Pacific Exploratory Missions (PEMs): PEM-West A, September-October 1991 in the western Pacific; PEM-West B, February-March 1994 in the western Pacific; and PEM-Tropics A, September-October 1996 in the central and eastern Pacific. PEM-Tropics A added measurements from the NASA P3-B aircraft. We used a new mode-based method to define a background against which to find layers. Using only O_3 and H_2O, we found 472 layers in PEM-Tropics A (0.72 layers per vertical kilometer profiled), 237 layers in PEM-West A (0.54 layers/km), and 158 layers in PEM-West B (0.41 layers/km). Using all constituents, we found 187 layers in PEM-Tropics A (0.43 layers/km), 128 layers in PEM-West A (0.29 layers/km), and 80 layers in PEM-West B (0.21 layers/km). Stratospheric air, sometimes mixed with trapped pollution, was the dominant layer source in all three missions. The larger number of layers per kilometer in PEM-Tropics A was probably due to repeated profiling of several "superlayers" visible in many of the mission lidar and potential vorticity profiles. The thickness of the superlayers was of order 1 km, and the horizontal extent was of order 1000 km. We found that layers have an important effect on the thermal structure. An example based on ozonesonde data from Tahiti is shown, where a dry, subsiding layer was stabilized by much greater radiative cooling at the base than at the top. The stabilized layer can trap pollution and force vertical plumes to spread into horizontal layers.

1. Introduction

Several plausible mechanisms for producing tropospheric layers exist. One mechanism is intruding stable stratospheric air, which then spreads out horizontally into the troposphere. Another mechanism is convection lifting air in a buoyant plume until it reaches its neutral buoyancy level and spreads out horizontally, as in the case of cumulus clouds. A large fire can produce a buoyant plume, similarly forming a layer. Large-scale subsidence can produce dry layers. Finally, layers with different chemical constituent mixing ratios can form due to a wind shear superimposing air masses from two very different source regions. In this paper we attempt to identify the predominant generating mechanism for certain layer types.

We collected observations from aircraft descending and ascending while measuring ozone, water vapor, carbon monoxide, methane, and other gases. We then used these trace constituent measurements to explore the altitudes, thickness, and frequencies of the layers so defined. The magnitudes of the trace constituent deviations within layers relative to their background values were also recorded and summarized. Taken together, this information allowed us to determine with some confidence the mechanisms important for layer creation. Data from three NASA missions [*Hoell et al.*, 1996, 1997], Pacific Exploratory Missions-West A and B (PEM-West A and B) and Pacific Exploratory Mission-Tropics A (PEM-Tropics A), were used. Both PEM-West missions were conducted in the western Pacific. PEM-West A was conducted in September and October 1991, a time of high convective activity, while PEM-West B took place in February and March 1994, a time of reduced convective activity. Thus comparing the layer types and frequencies defined in the latter two missions allows us to determine the relative importance of convection and trapping by stratospheric air on layer formation. *Newell et al.* [1996] reported PEM-West A layers, and *Wu et al.* [1997] reported PEM-West B layers; layers from another aircraft mission were reported by *Collins et al.* [1996a]. PEM-Tropics A took place in September-October 1996, sampling the central and eastern Pacific. This is a completely different region, suspected to be much less influenced by anthropogenic emissions and characterized by different dynamical features. We used our analysis to shed light on these differences by comparing the layer structure found in PEM-Tropics A to that in PEM-West. Determining the effect of urban and industrial pollution and, more importantly, biomass burning, in South America, New Zealand, Indonesia, Australia, and possibly even Africa, on this region is also very important.

[1]Department of Earth, Atmospheric, and Planetary Sciences, Massachusetts Institute of Technology, Cambridge.

[2]Laboratoire d'Aérologie, CNRS, Toulouse, France.

[3]Department of Atmospheric, Oceanic, and Space Sciences, University of Michigan, Ann Arbor.

[4]NASA Langley Research Center, Hampton, Virginia.

[5]School of Earth and Atmospheric Science, Georgia Institute of Technology, Atlanta.

[6]Deceased, June 16, 1997.

PEM−WEST FLIGHT ROUTES
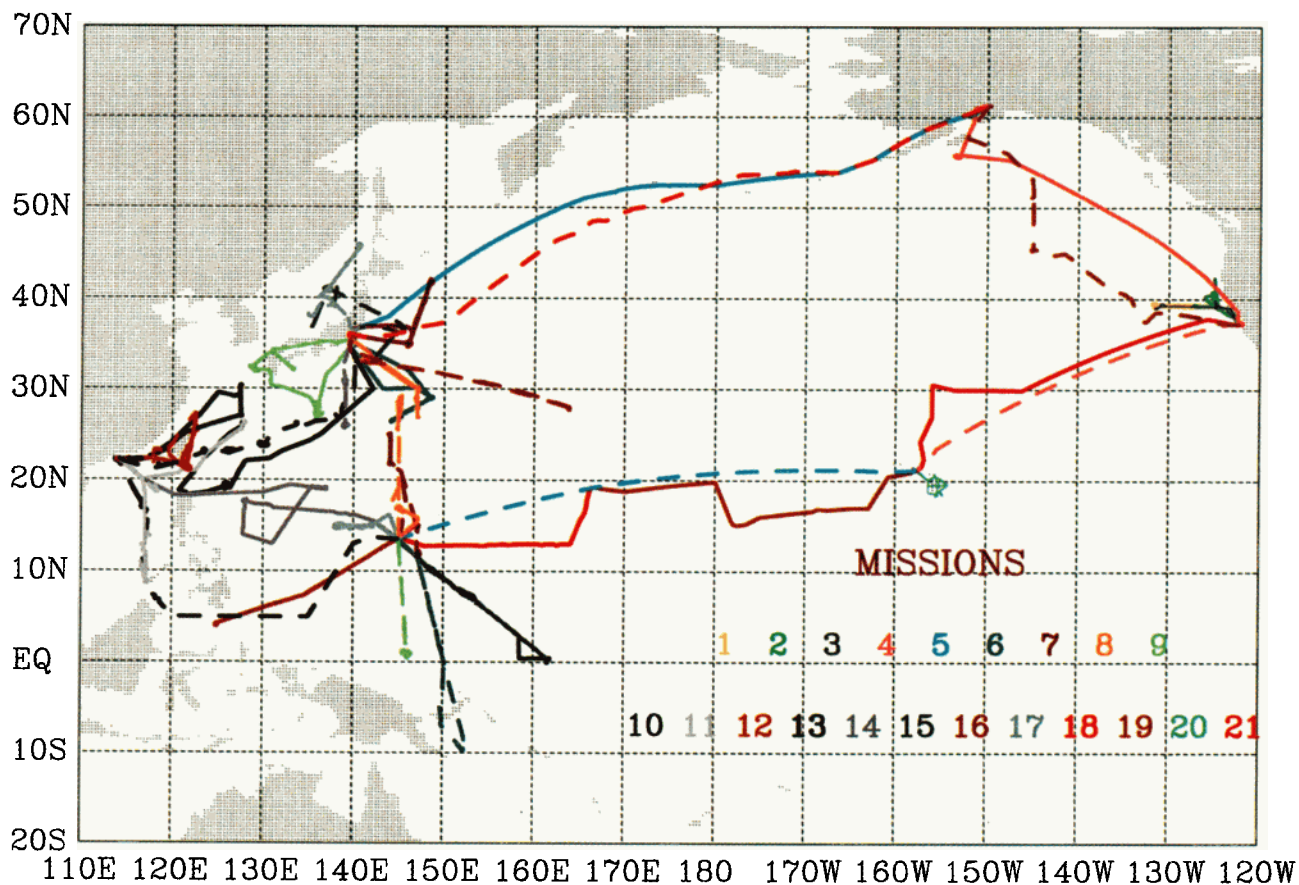### SOLID FOR A, DASHED FOR B

Plate 1a. Map of the NASA DC-8 flight tracks during PEM-West A. Each flight track is in the color of the flight number. Map of the NASA DC-8 flight tracks during PEM-West B. Each flight track is in the color of the flight number.

2. Data and Procedures

Plate 1a shows the flight path of the NASA DC-8 during PEM-West A and PEM-West B. Plate 1b shows the flight path of the NASA DC-8 and P-3B during PEM-Tropics A. We analyzed data from PEM-West A flights 4-21, PEM-West B flights 4-19, PEM-Tropics A DC-8 flights 4-16, 18, 19, and P-3B flights 6-20. During each flight the aircraft measured a vertical profile during takeoff and landing, and again during the course of almost all flights. We analyzed those profiles that sampled at least 2.5 vertical kilometers without interruption by any level flight segments. In PEM-West A, 88 such profiles were made, while 84 were made in PEM-West B. In PEM-Tropics A the DC-8 made 86 such profiles and the P3-B made 72. For comparison purposes, we divided the number of layers in any category for each mission by the total number of vertical kilometers summed over all profiles analyzed for each mission. The distribution of kilometers sampled into altitude bins does not vary much from mission to mission and from altitude level to altitude level, except for reduced sampling above about 8 km. In comparing the results from the three missions, we discuss tropospheric layered structure from 2 to 10 km and ignore any bias possibly

introduced by the slight unevenness in the sampling. The location of the flight tracks (Plates 1a-1b) may also have had some effect on the average layered structure of the regions and time periods sampled.

Most of the vertical profiles were altitude ramps covering horizontal distances between 100 and 200 km; some were spirals near the same horizontal position. We note that profiles taken over 100 to 200 km may identify spurious layers that were actually vertical plumes; however, comparing the profiles with ozone mixing ratio lidar images (see below) shows that the detected deviations had a significant horizontal extent and are best identified as horizontal layers.

The missions used fast response instruments to measure O_3, H_2O, CO, and CH_4 mixing ratios. Ozone was measured on the DC-8 with a nitric oxide chemiluminescence technique [*Gregory et al.*, 1987] with a time resolution of 2 Hz. On the P3-B, ozone was measured by M. Carroll with a time resolution of 1 Hz, also using nitric oxide chemiluminescence. On both aircraft, carbon monoxide and methane were measured with a mid-IR diode laser instrument using a differential absorption technique [*Collins et al.*, 1996b; *Sachse et al.*, 1987]. Three different instruments to measure water vapor were used in the mission. In PEM-Tropics A only, the DC-8

PEM–TROPICS FLIGHT ROUTES
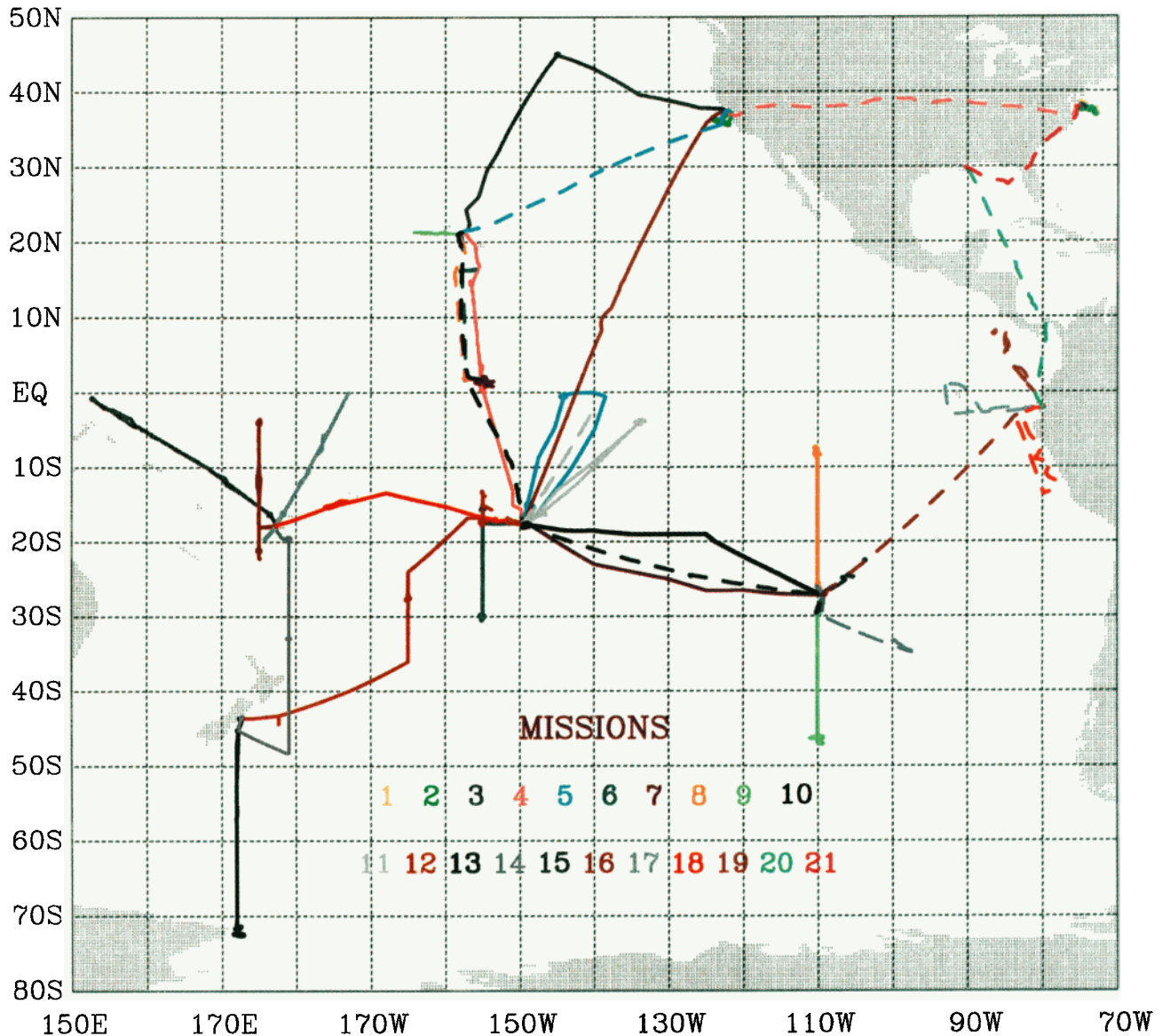## SOLID FOR DC8, DASHED FOR P3B

Plate 1b. Map of the NASA DC-8 flight tracks during PEM-Tropics A. Each flight track is in the color of the flight number. Map of the NASA P-3B flight tracks during PEM-Tropics A. Each flight track is in the color of the flight number.

carried an instrument to measure water vapor mixing ratios using an external path diode laser. In PEM-West A the DC-8 carried a Lyman-α fluorescence hygrometer. Both the external path diode laser instrument (for all mixing ratios) and the Lyman-α fluorescence instrument (for mixing ratios < 0.5g/kg) were more accurate than the General Eastern Model 1011B dew/frost point hygrometer used in all of the missions. Data from the diode laser hygrometer were used to find layers in all PEM-Tropics A DC-8 vertical profiles except flight 4, flight 6, and flight 16, where it was unavailable; we used the General Eastern Model 1011B dew/frost point hygrometer for the P3-B and the DC-8 in PEM-Tropics A flights 4, 6, and 16. Data from the dew/frost point hygrometer were used for the PEM-

Tropics A P3-B profiles, the PEM-West B profiles, and the PEM-West A profiles for mixing ratios ≥ 0.5 g/kg. Data from the Lyman-α instrument were used for the PEM-West A profiles for mixing ratios < 0.5g/kg. We used PEM-West A data with a 10-s time resolution, PEM-West B data with a 5-s time resolution, and PEM-Tropics A data with a time resolution of 1-s for O_3 and H_2O, and 5 s for CO and CH_4.

On the basis of an extensive visual analysis of time series plots and altitude profiles of the various constituents, we found that the O_3, CO, and CH_4 background levels remained fairly constant with altitude throughout the troposphere. The significant exception was the marine boundary layer, where O_3, CO, and CH_4 mixing ratios were generally significantly

Table 1. Different Possible Mechanisms for Layer Production and the Expected Trace Constituent Compositions

Tracer	Mechanism
$+O_3$ $+H_2O$ $+CO$ $+CH_4$	polluted air raised by convection
$+O_3$ $-H_2O$ $+CO$ $+CH_4$	polluted air (may have a stratospheric cap)
$+O_3$ $-H_2O$ $-CO$ $-CH_4$	stratospheric air
$+O_3$ $-H_2O$ $+CO$ $-CH_4$	urban/industrial pollution
$+O_3$ $-H_2O$ $-CO$ $+CH_4$	aged pollution
$-O_3$ $-H_2O$ $-CO$ $-CH_4$	clean, subsiding marine air
$-O_3$ $+H_2O$ $-CO$ $-CH_4$	clean air raised from the boundary layer by convection

Plus refers to a positive deviation from the background. Minus refers to a negative deviation from the background.

lower than in the free troposphere, due to more abundant OH in this moist region. We neglected the lowest 2 km of the atmosphere to avoid defining the marine boundary layer as a layer in our statistics while recognizing that this approach may introduce a bias against these lower mixing ratios.

We now outline the procedure used for defining the constituent background. First, we eliminated any linear trend present in the profile by subtracting out the least squares fit to a straight line. Then we divided the resultant data into bins of width 10 ppbv (10% relative humidity for H_2O). Then a straight line was fitted in a least squares sense to the data points in the bin with the most points (the mode). Finally, the linear trend of the original profile was added back. If fewer than 25% of the data points were in the mode bin, then it was deemed to be an ill-defined mode, and the background was defined simply by the original straight line fitted to the profile. Unreasonably low or high values of the background were avoided by bounding them between the minimum and maximum values in the data profile, as well as with hard limits for maximum possible background values of O_3, CO, and CH_4 of 80, 150, and 1770 ppbv, and a minimum possible background value for relative humidity of 10%. Relative humidity was used instead of specific humidity for water vapor because the rapid decrease of the latter with height did not work well with the mode-based definition of a background profile.

The layer detection criteria were as follows. For each O_3 data point with a deviation from the background exceeding 5 ppbv, if we could find a point above and below it with a deviation less than 2.5 ppbv, we defined a layer stretching between these two latter points. Layers for the other constituents were defined by searching the altitude interval between point A and point B for deviations from the background greater than 5% (relative humidity) or 3 ppbv (CO and CH_4), where A was halfway between the height of

maximum O_3 deviation and the beginning height of the O_3 layer, and B was halfway between the height of the maximum O_3 deviation and the ending height of the O_3 layer.

One of the key objectives of PEM was to study the ozone budget over the Pacific. This is why we used ozone as the first criterion for defining a layer. We focused on identifying polluted and stratospheric layers where ozone production has occurred or is occurring, and layers where ozone is destroyed, for example, marine air exposed to high levels of ultraviolet radiation. Thus, though it would be possible to define a layer category in which the ozone level is close to background, we only examined layers with ozone mixing ratios well above or well below the background. Once we found ozone layers semiobjectively using our algorithm, we looked at other constituents to determine the possible mechanisms through which the layer was created. We used water vapor as a second criterion because it is a good way to determine whether a layer was produced by subsidence (low water vapor) or convection (high water vapor). One ambiguity is that polluted air is frequently low in water vapor because it originated over the continents rather than over the ocean but does not necessarily form layers through subsidence. In order to distinguish between pollution and subsiding stratospheric air, both of which are high in ozone and low in water vapor, we looked for high CO and CH_4 mixing ratios as additional markers of pollution. Stratospheric air would have high ozone but CO and CH_4 mixing ratios below the background level. Even the use of all four trace constituents does not completely distinguish stratospheric and polluted air; the high stability of stratospheric air allows it to trap pollution. We used lidar and potential vorticity data to resolve this problem as described below.

Layers with O_3, CO, and CH_4 mixing ratios below the background level have been photochemically cleansed, usually in the marine boundary layer. If such layers are H_2O-

Table 2a. PEM-Tropics A Statistics of the Layers Based on O_3 and H_2O

Type	Tracer	Obs	Percent	Obs/kilometer	h, km	p, hPa	Δh, km	Δp, hPa	ΔO_3, ppbv	ΔH_2O, %
1	$+H_2O$ $+O_3$	43	9	0.07	5.5	536	0.36	24	14	19
2	$-H_2O$ $+O_3$	245	52	0.37	5.2	562	0.56	41	13	-18
3	$+H_2O$ $-O_3$	85	18	0.13	5.2	575	0.45	33	-10	21
4	$-H_2O$ $-O_3$	99	21	0.15	5.6	531	0.37	24	-9	-16
Total or mean		472		0.72	5.2	556	0.49	34	12	18

Total kilometers of ascent and descent checked for layers: 654.8 km. Abbreviations in the table are obs, number of observed layers; percent, percentage of obs in total; obs/kilometer, ratio of observed layers per kilometer; h and p, mean altitude and pressure of the layers; Δh and Δp, mean depth in units of kilometers and hectopascals; ΔO_3 and ΔH_2O, O_3 and relative humidity deviations from background (as defined in text).

Table 2b. PEM-West A Statistics of the Layers Based on O_3 and H_2O

Type	Tracer	Obs	Percent	Obs/kilometer	h, km	p, hPa	Δh, km	Δp, hPa	ΔO_3, ppbv	ΔH_2O, %
1	$+H_2O +O_3$	58	24	0.13	5.6	517	0.57	39	10	16
2	$-H_2O +O_3$	101	43	0.23	5.3	536	0.61	42	12	-17
3	$+H_2O -O_3$	42	18	0.10	5.7	509	0.55	38	-8	22
4	$-H_2O -O_3$	36	15	0.08	5.6	511	0.70	46	-11	-16
Total or mean		237		0.54	5.5	523	0.60	41	10	18

Total kilometers of ascent and descent checked for layers: 438.7 km. Abbreviations in the table are obs, number of observed layers; percent, percentage of obs in total; obs/kilometer, ratio of observed layers per kilometer; h and p, mean altitude and pressure of the layers; Δh and Δp, mean depth in units of kilometers and hectopascals; ΔO_3 and ΔH_2O, O_3 and relative humidity deviations from background (as defined in text).

rich, they were probably raised from the boundary layer by convection. Because the convective layers generally spread out horizontally at close to the tropopause level, we did not expect to see many such layers; the DC-8 can only sample up to about 12 km and the P3-B can only sample up to about 8 km. If O_3-, CO-, and CH_4-poor layers are also H_2O poor, then they probably underwent subsidence after convection raised them from a clean boundary layer region. Layers with high O_3, high CO, and low CH_4 mixing ratios are probably caused by urban or industrial pollution. While CH_4 is released by biomass burning, it is often present in anthropogenic pollution, too, from enteric fermentation, rice paddies, landfills, animal waste, and domestic sewage, these together totaling about 6 times the amount from biomass burning [e.g., see Intergovernmental Panel on Climate Change (*IPCC*), 1995]. Elevated O_3 and CH_4 levels and low CO levels may suggest older polluted air, as CO is photochemically destroyed faster than CH_4. We suspect that layers high in all constituents, including water vapor, originate from pollution raised by convective activity. It is also possible that some of the elevated constituent levels (O_3, CO) are due to chemical reactions in lightning strokes [*Boldi*, 1992]. Our method of identifying the mechanism through which ozone rich and ozone poor layers are formed dynamically is summarized in Table 1. We indicate layers with high levels of a given constituent by writing a plus before the constituent and layers with low levels by writing a minus before the constituent.

Two previous papers on layers [*Newell et al.*, 1996; *Wu et al.*, 1997] used a different algorithm to identify layers from the PEM-West A and PEM-West B flights. Because of significant problems with overestimation of the layer number by the original algorithm, we used our new algorithm to analyze the results from PEM-Tropics A and to reanalyze those from PEM-West.

3. Layers Defined by Ozone and Water Vapor

We will refer to ozone rich and water vapor rich ($+O_3 +H_2O$) layers as type 1 layers, ozone rich and water vapor poor ($+O_3 -H_2O$) layers as type 2, ozone poor and water vapor rich ($-O_3 +H_2O$) layers as type 3, and ozone poor and water vapor poor ($-O_3 -H_2O$) layers as type 4. The results are summarized in Tables 2a-2c. On the basis of these two criteria alone, we found 472 layers in 158 PEM-Tropics A profiles covering 655 vertical kilometers, 237 layers in 88 PEM-West A profiles covering 439 km, and 158 layers in 84 PEM-West B profiles covering 388 km. This corresponds to 0.72 layers/km in PEM-Tropics A, 0.54 layers/km in PEM-West A, and 0.41 layers/km in PEM-West B. We obtained the fraction of the atmosphere composed of layers with high or low ozone and water vapor by multiplying the number of layers per kilometer by the mean layer depth. This gives 0.35 for PEM-Tropics A, 0.32 for PEM-West A, and 0.26 for PEM-West B. (Note that PEM-Tropics A had thinner layers on the average, which probably means that the finer resolution of the data from that mission enabled us to "see" the thinner structures missed out in the previous missions.) Given the geographical difference between PEM-Tropics A and PEM-West, and the meteorological and seasonal differences between PEM-West A and PEM-West B, the similarity is surprising. The similarity allows us to tentatively suggest that the various mechanisms producing layers (Table 1) have the same effect in different seasons and in different regions of the Pacific. Only the thickness, altitude, CO, CH_4, and probably other trace constituent mixing ratios change.

The layer statistics are summarized graphically in Figure 1. This figure shows the overwhelming dominance of type 2 layers in all three missions. Table 1 reveals that this could be attributed to any combination of stratospheric or polluted air. Figures 2a-2d demonstrate how the centers of these layers are

Table 2c. PEM-West B Statistics of the Layers Based on O_3 and H_2O

Type	Tracer	Obs	Percent	Obs/kilometer	h, km	p, hPa	Δh, km	Δp, hPa	ΔO_3, ppbv	ΔH_2O, %
1	$+H_2O +O_3$	14	9	0.04	5.8	495	0.67	46	12	24
2	$-H_2O +O_3$	87	55	0.22	5.7	500	0.68	46	15	-23
3	$+H_2O -O_3$	16	10	0.04	5.2	546	0.65	47	-13	21
4	$-H_2O -O_3$	41	26	0.11	5.9	489	0.54	36	-8	-21
Total or mean		158		0.41	5.7	502	0.64	43	13	22

Total kilometers of ascent and descent checked for layers: 387.6 km. Abbreviations in the table are obs, number of observed layers; percent, percentage of obs in total; obs/kilometer, ratio of observed layers per kilometer; h and p, mean altitude and pressure of the layers; Δh and Δp, mean depth in units of kilometers and hectopascals; ΔO_3 and ΔH_2O, O_3 and relative humidity deviations from background (as defined in text).
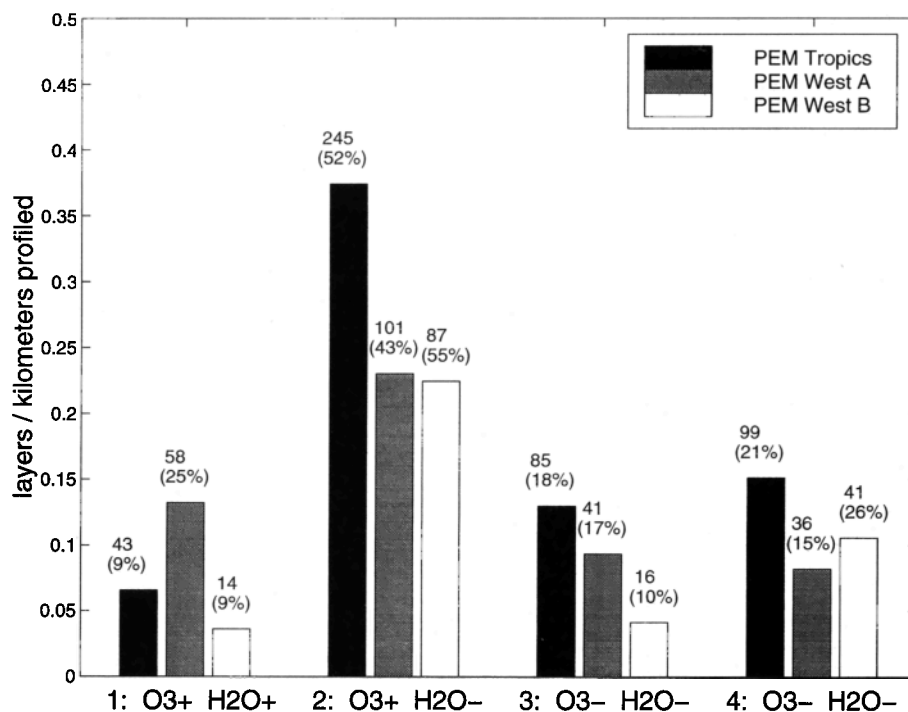
Figure 1. Number of layers detected per kilometer profiled. Layers are defined by O_3 and H_2O deviations.

distributed into altitude bins. Tables 3a-3c summarize the layer characteristics of layers in each altitude bin. We note here that the term "number of layers" will refer to the number of layers per kilometer sampled. We thus use the number of layers per kilometer as a measure of the actual layer number present in the sampling regions during the mission periods. The maximum number of layers was found between 4 and 8 km

for all missions. The distribution of layers with height was fairly constant across the missions, again providing evidence for the universal nature of layer occurrence. The plots in Figures 2a-2d have been normalized by the number of kilometers profiled in each mission, so these results are not sampling artifacts. We note again that the somewhat higher number of layers detected during PEM-Tropics A is mostly
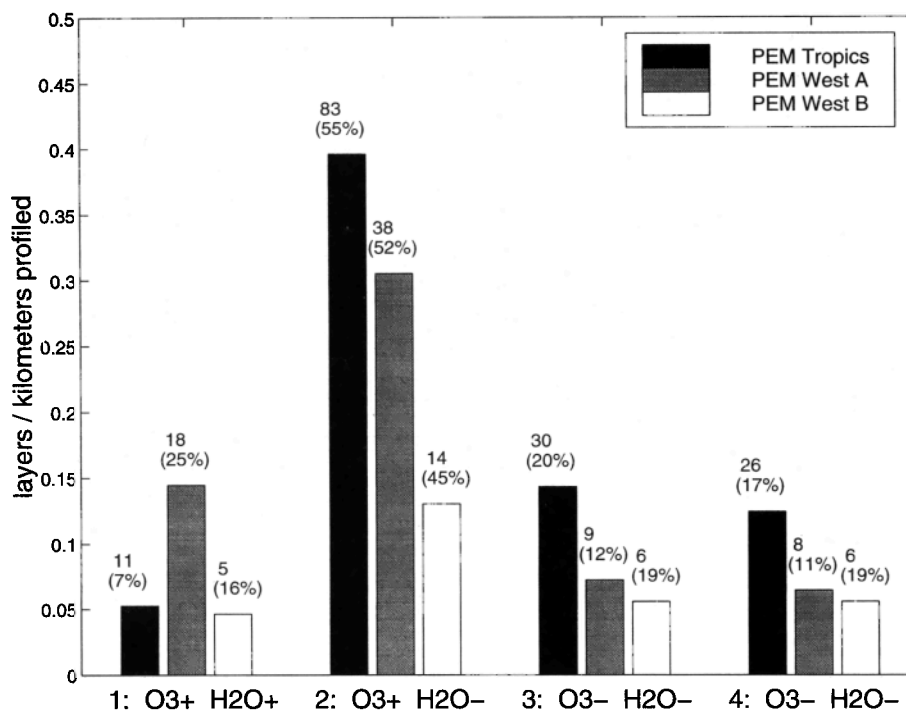

Figure 2a. Number of layers detected per kilometer profiled between 2 and 4 km. Layers are defined by O_3 and H_2O deviations.
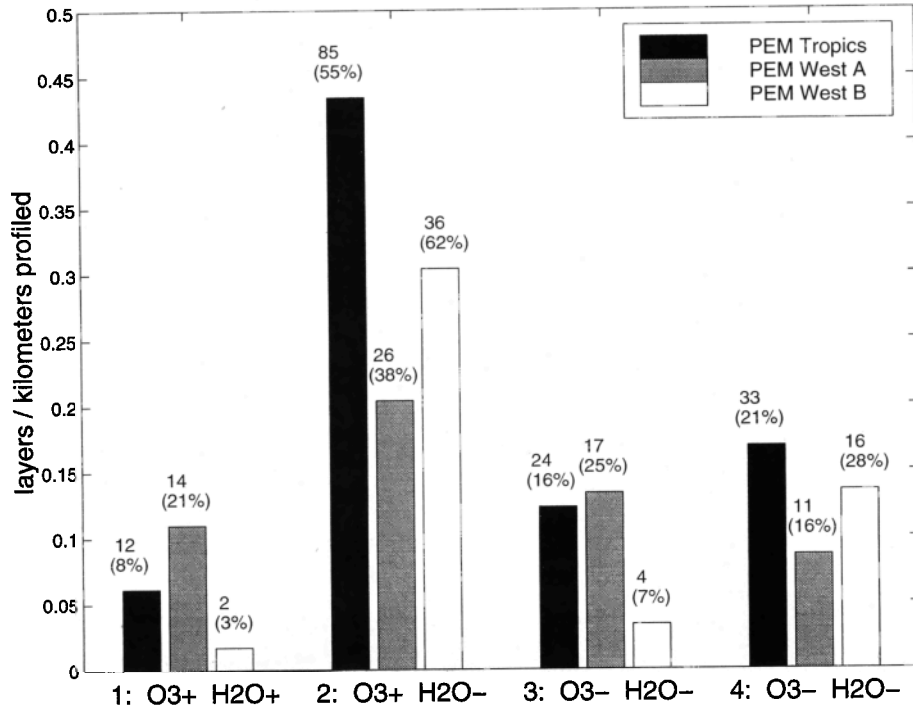
Figure 2b. Number of layers detected per kilometer profiled between 4 and 6 km. Layers are defined by O_3 and H_2O deviations.

offset by the lower value of the mean layer thickness, which was probably due to the higher resolution of the PEM-Tropics A data.

From Tables 2a-2c one can glean the differences in the distribution of O_3-H_2O layer types between missions. As noted before, type 2 was dominant for all missions. This will be discussed further in the next section where the other constituents will be taken into account. PEM-West A had a significantly larger percentage of type 1 layers, which is consistent with the presence of strong convection over Asia (convection plus pollution) during that period. On the other hand, PEM-West B had more of type 4 and less of type 3, which fits the general picture of widespread subsidence over the ocean during that mission.
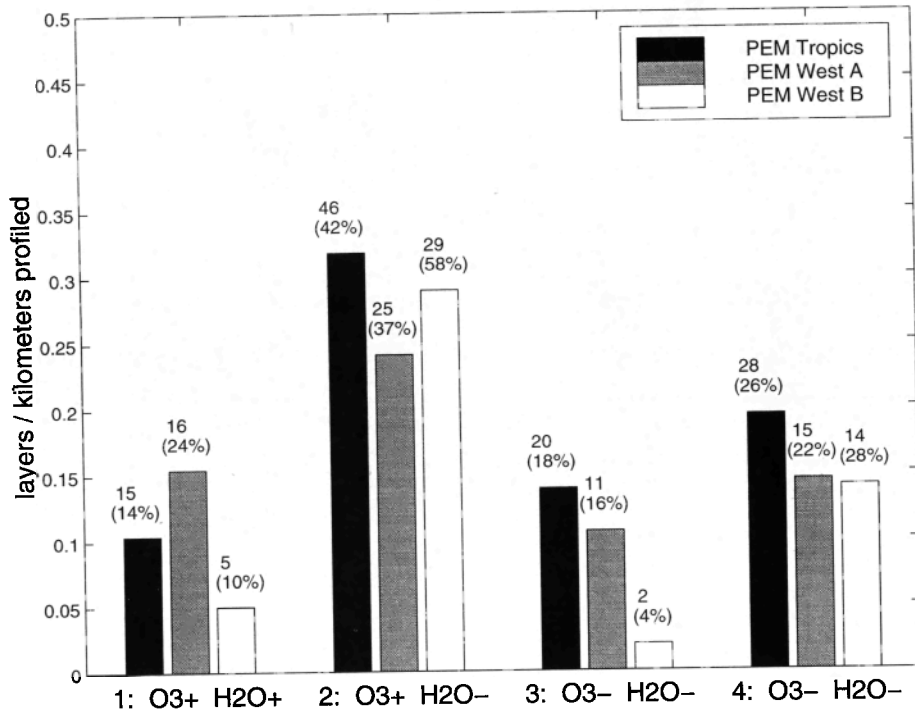

Figure 2c. Number of layers detected per kilometer profiled between 6 and 8 km. Layers are defined by O_3 and H_2O deviations.
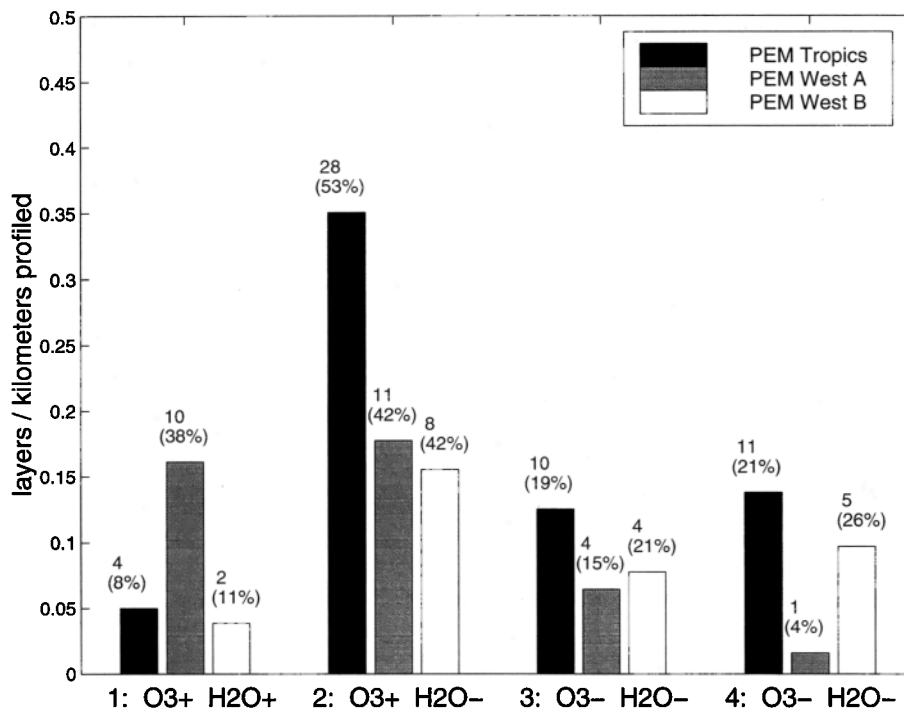
Figure 2d. Number of layers detected per kilometer profiled between 8 and 10 km. Layers are defined by O_3 and H_2O deviations.

4. Layers Defined by Ozone, Water Vapor, Carbon Monoxide, and Methane

We expanded the definition of type 1-4 layers above by appending the letter A for $+CO$ $+CH_4$ layers, B for $+CO$ $-CH_4$ layers, C for $-CO$ $+CH_4$ layers, and D for $-CO$ $-CH_4$ layers. Tables 4a-4c show the layer statistics based on all four criteria for the three missions; Figure 3 illustrates the number of layers per kilometer for each layer type. This figure shows that ozone-rich, water-vapor-poor (type 2) layers dominate. In PEM-Tropics A, 87% of these layers were polluted (type 2a), and 13% were stratospheric (type 2d); in PEM-West A, 96% were polluted and 4% were stratospheric; and in PEM-West B, 70% were polluted, and 30% were stratospheric. The dominance of polluted type 2 layers across all missions points to the importance of atmospheric stability working against buoyant convection in layer formation. Plausible scenarios are layers of stratospheric intrusions trapping rising polluted air, and pollution plumes rising to a high level where they become neutrally buoyant and spread out like anvils. In

PEM-West B the widespread subsidence helping prevent pollution from escaping the boundary layer was probably responsible for the lower percentage of polluted type 2 layers.

The average layer characteristics, obviously dominated by type 2 layers, vary from mission to mission. Because no

Table 3b. PEM-West A Changes of Statistics of Layers With Height

Height, km	Obs	Obs/ kilometer	h, km	p, hPa	Δh, km	Δp, hPa	ΔO_3, ppbv	ΔH_2O, %
2–4	73	0.59	3.2	688	0.5	40	10	16
4–6	68	0.53	5.0	544	0.6	43	10	20
6–8	67	0.65	7.0	412	0.8	47	12	18
8–10	26	0.42	8.7	320	0.5	25	10	16
10–12	2	0.11	10.5	247	0.9	35	8	28

Abbreviations in the table are obs, number of observed layers; obs/kilometer, ratio of observed layers per kilometer; h and p, mean altitude and pressure of the layers; Δh and Δp, mean depth in units of kilometers and hectopascals; ΔO_3 and ΔH_2O, O_3 and relative humidity deviations from background (as defined in text).

Table 3a. PEM-Tropics A Changes of Statistics of Layers With Height

Height, km	Obs	Obs/ kilometer	h, km	p, hPa	Δh, km	Δp, hPa	ΔO_3, ppbv	ΔH_2O, %
2–4	150	0.72	3.1	727	0.4	35	11	19
4–6	154	0.79	5.0	564	0.5	36	12	18
6–8	109	0.75	6.9	440	0.6	35	13	19
8–10	53	0.66	8.8	317	0.5	28	12	13
10–12	6	0.24	10.5	243	0.5	18	7	16

Abbreviations in the table are obs, number of observed layers; obs/kilometer, ratio of observed layers per kilometer; h and p, mean altitude and pressure of the layers; Δh and Δp, mean depth in units of kilometers and hectopascals; ΔO_3 and ΔH_2O, O_3 and relative humidity deviations from background (as defined in text).

Table 3c. PEM-West B Changes of Statistics of Layers With Height

Height, km	Obs	Obs/ kilometer	h, km	p, hPa	Δh, km	Δp, hPa	ΔO_3, ppbv	ΔH_2O, %
2–4	31	0.29	3.3	675	0.6	48	10	24
4–6	58	0.49	5.0	544	0.6	42	11	23
6–8	50	0.50	7.0	411	0.8	50	16	22
8–10	19	0.37	8.6	325	0.4	21	11	22
10–12	0	0	—	—	—	—	—	—

Abbreviations in the table are obs, number of observed layers; obs/kilometer, ratio of observed layers per kilometer; h and p, mean altitude and pressure of the layers; Δh and Δp, mean depth in units of kilometers and hectopascals; ΔO_3 and ΔH_2O, O_3 and relative humidity deviations from background (as defined in text).

Table 4a. PEM-Tropics A Statistics of the Layers Based on O_3, H_2O, CO, and CH_4

Type	Tracer	Obs	Percent	h, km	p, hPa	Δh, km	Δp, hPa	ΔO_3, ppbv	ΔH_2O, %	ΔCO, ppbv	ΔCH_4, ppbv
1A	$+O_3+H_2O+CO+CH_4$	15	8	6.4	461	0.56	34	21	20	23	12
1B	$+O_3+H_2O+CO-CH_4$	0	0	—	—	—	—	—	—	—	—
1C	$+O_3+H_2O-CO+CH_4$	1	1	2.2	775	0.17	16	10	28	-3	3
1D	$+O_3+H_2O-CO-CH_4$	3	2	6.3	509	0.25	12	10	15	-10	-6
2A	$+O_3-H_2O+CO+CH_4$	60	32	5.3	561	0.96	68	20	-20	13	12
2B	$+O_3-H_2O+CO-CH_4$	12	6	4.8	598	1.01	73	17	-17	17	-6
2C	$+O_3-H_2O-CO+CH_4$	12	6	6.2	475	0.79	56	15	-14	-8	7
2D	$+O_3-H_2O-CO-CH_4$	13	7	5.1	579	0.56	39	15	-15	-11	-11
3A	$-O_3+H_2O+CO+CH_4$	11	6	4.4	654	0.35	31	-9	23	22	9
3B	$-O_3+H_2O+CO-CH_4$	9	5	4.8	612	0.54	42	-13	19	19	-9
3C	$-O_3+H_2O-CO+CH_4$	3	2	5.4	537	1.23	76	-13	25	-7	4
3D	$-O_3+H_2O-CO-CH_4$	13	7	5.4	542	0.55	37	-13	24	-13	-7
4A	$-O_3-H_2O+CO+CH_4$	9	5	4.2	641	0.32	27	-8	-14	22	9
4B	$-O_3-H_2O+CO-CH_4$	5	3	5.6	559	0.44	27	-13	-16	8	-11
4C	$-O_3-H_2O-CO+CH_4$	3	2	7.0	465	1.02	55	-11	-17	-16	8
4D	$-O_3-H_2O-CO-CH_4$	18	10	6.3	495	0.55	34	-11	-16	-16	-12
Total or mean		187		5.4	553	0.71	50	16	19	15	10

Abbreviations in the table are obs, number of observed layers; percent, percentage of obs in total; h and p, mean altitude and pressure of the layers; Δh and Δp, mean depth in units of kilometers and hectopascals; ΔO_3 and ΔH_2O, O_3 and relative humidity deviations from background (as defined in text); ΔCO and ΔCH_4, CO, and CH_4 deviations from background (as defined in text).

algorithm is foolproof for detecting layers, categories that have only a small number of layers should be treated as statistical noise. The only other layer types that our analysis suggests may be important are the type 1A and 4D layers. The first is high in all of the constituents and is probably produced by convection raising polluted air to a neutral buoyancy level. This type was most significant during PEM-West A, which, as noted before, is consistent with the presence of strong convection over Asia during that time.

Though the ozone deviation from the background was between 13 and 16 ppbv for all three missions (Tables 4a-4c),

the average CO deviation was much higher in PEM-West B than in the other missions. This was likely due to the maximization of the outflow of continental air from Asia carrying high levels of industrial pollution during the PEM-West B period. At the same time, polluted layers in PEM-West had more elevated CH_4 than in PEM-Tropics A, suggesting that the southern hemisphere pollution sampled was diluted more than the northern hemisphere pollution. Because of the low number of samples in the other layer categories, we hesitate to make any comparison between missions. Without further sampling, we can only say that

Table 4b. PEM-West A Statistics of the Layers Based on O_3, H_2O, CO, and CH_4

Type	Tracer	Obs	Percent	h, km	p, hPa	Δh, km	Δp, hPa	ΔO_3, ppbv	ΔH_2O, %	ΔCO, ppbv	ΔCH_4, ppbv
1A	$+O_3+H_2O+CO+CH_4$	16	12	5.8	501	0.56	37	13	15	13	27
1B	$+O_3+H_2O+CO-CH_4$	0	0	—	—	—	—	—	—	—	—
1C	$+O_3+H_2O-CO+CH_4$	6	5	6.0	478	0.87	61	12	22	-9	18
1D	$+O_3+H_2O-CO-CH_4$	3	2	6.5	438	0.57	34	8	7	-7	-11
2A	$+O_3-H_2O+CO+CH_4$	31	24	5.6	515	0.81	53	15	-18	12	19
2B	$+O_3-H_2O+CO-CH_4$	4	3	5.9	491	0.43	25	12	-26	14	-7
2C	$+O_3-H_2O-CO+CH_4$	17	13	5.1	538	0.60	42	15	-18	-16	21
2D	$+O_3-H_2O-CO-CH_4$	2	2	5.3	516	0.29	21	9	-15	-5	-10
3A	$-O_3+H_2O+CO+CH_4$	10	8	6.8	438	0.67	40	-10	19	13	36
3B	$-O_3+H_2O+CO-CH_4$	4	3	5.7	508	0.46	36	-11	25	19	-15
3C	$-O_3+H_2O-CO+CH_4$	3	2	6.5	452	0.62	44	-6	15	-7	5
3D	$-O_3+H_2O-CO-CH_4$	6	5	4.7	576	1.09	74	-7	32	-11	-12
4A	$-O_3-H_2O+CO+CH_4$	7	5	5.8	505	0.75	49	-10	-16	17	38
4B	$-O_3-H_2O+CO-CH_4$	2	2	6.8	421	1.37	83	-13	-18	16	-11
4C	$-O_3-H_2O-CO+CH_4$	4	3	5.6	500	0.87	58	-12	-14	-12	10
4D	$-O_3-H_2O-CO-CH_4$	13	10	5.5	515	0.76	51	-12	-16	-14	-16
Total or mean		128		5.7	505	0.72	47	13	18	13	20

Abbreviations in the table are obs, number of observed layers; percent, percentage of obs in total; h and p, mean altitude and pressure of the layers; Δh and Δp, mean depth in units of kilometers and hectopascals; ΔO_3 and ΔH_2O, O_3 and relative humidity deviations from background (as defined in text); ΔCO and ΔCH_4, CO, and CH_4 deviations from background (as defined in text).

Table 4c. PEM-West B Statistics of the Layers Based on O_3, H_2O, CO, and CH_4

Type	Tracer	Obs	Percent	h, km	p, hPa	Δh, km	Δp, hPa	ΔO_3, ppbv	ΔH_2O, %	ΔCO, ppbv	ΔCH_4, ppbv
1A	$+O_3+H_2O+CO+CH_4$	3	4	5.5	509	1.30	85	14	34	69	10
1B	$+O_2+H_2O+CO–CH_4$	4	5	6.6	442	0.49	33	13	34	48	–5
1C	$+O_2+H_2O–CO+CH_4$	0	0	—	—	—	—	—	—	—	—
1D	$+O_2+H_2O–CO–CH_4$	0	0	—	—	—	—	—	—	—	—
2A	$+O_2–H_2O+CO+CH_4$	19	24	5.3	530	0.58	41	11	–25	33	17
2B	$+O_2–H_2O+CO–CH_4$	4	5	6.8	424	1.86	120	23	–19	11	–12
2C	$+O_2–H_2O–CO+CH_4$	9	11	5.2	537	0.58	43	11	–22	–12	14
2D	$+O_2–H_2O–CO–CH_4$	14	18	6.6	440	0.84	54	27	–25	–18	–14
3A	$–O_2+H_2O+CO+CH_4$	5	6	4.7	581	0.69	55	–12	28	27	13
3B	$–O_2+H_2O+CO–CH_4$	0	0	—	—	—	—	—	—	—	—
3C	$–O_2+H_2O–CO+CH_4$	1	1	4.7	561	0.84	61	–34	18	–4	10
3D	$–O_2+H_2O–CO–CH_4$	1	1	5.1	534	0.47	34	–15	13	–16	–5
4A	$–O_2–H_2O+CO+CH_4$	8	10	5.7	496	0.72	50	–6	–20	38	22
4B	$–O_2–H_2O+CO–CH_4$	2	2	6.0	477	0.40	23	–10	–22	4	–3
4C	$–O_2–H_2O–CO+CH_4$	3	4	5.8	494	0.66	43	–12	–10	–5	7
4D	$–O_2–H_2O–CO–CH_4$	7	9	4.7	576	0.67	47	–10	–14	–15	–14
Total or mean		80		5.6	506	0.74	51	14	23	25	14

Abbreviations in the table are obs, number of observed layers; percent, percentage of obs in total; h and p, mean altitude and pressure of the layers; Δh and Δp, mean depth in units of kilometers and hectopascals; ΔO_3 and ΔH_2O, O_3 and relative humidity deviations from background (as defined in text); ΔCO and ΔCH_4, CO, and CH_4 deviations from background (as defined in text).

these layer types are rare compared to the stratospheric/pollution type.

5. Some Characteristic Examples

One problem with detecting layers using measurements on an aircraft making a vertical profile is that it requires many vertical profiles over a large geographical area to obtain both the vertical and horizontal layer distribution. A better method for examining the horizontal extent is to use lidar profiles made below and above the aircraft. The DC-8 carried both an upward and a downward looking lidar to measure the ozone mixing ratio. Though the lidar resolution is not as good as the resolution of the vertical profiles made with the in situ instruments, it can be used in one direction to determine the horizontal extent of relatively thick (> 1 km) layers in ozone.

A thick layer in the ozone profile, with an ozone mixing ratio about 20 ppbv above background, was observed during the DC-8 flight 10 from Easter Island to Tahiti. The layer extended from 2.5 to 7.0 km in altitude at its thickest, and stretched horizontally from at least 23°S, 118°W to 18°S, 146.7°W, a distance exceeding 2000 km (Plate 2). It is possible that the lidar observed two different layers at similar altitudes, since there was a break in the layer where convection may have intruded between 19°S, 130°W and 19°S, 135°W. It is also possible that this break in the layer was only a thinning of the layer to a size that the lidar profile could not resolve. The layer was only about 1 km thick around 19°S, 135°W. This layer was profiled by the DC-8 during a descent around 2305 UT (144.6°W, 18.4°S). The layer was sampled between 4.4 and 5.6 km (Figure 4) and was found to have high ozone, carbon monoxide, and methane, and low water vapor; this was clearly polluted air. On the basis of the chemical constituents alone, we would identify this layer as having arisen from pollution, most likely biomass burning. However, a PV profile from European Centre for Medium-

Range Weather Forecasts (ECMWF) data showed intrusion of extremely stable stratospheric air into the troposphere at that level (Plate 3). The stratospheric air had probably acted as a cap to polluted air rising from the boundary layer. On the basis of an analysis of lidar and PV data for PEM-Tropics A, we conclude that many of the polluted layers were influenced by this mechanism.

The similarities between P3-B flight 12 ascent/descent 2 and DC-8 flight 6 ascent/descent 1 were striking. Compare the two vertical profiles in Figures 5 (DC-8) and 6 (P-3B). Both profiles show a peak in the water vapor at about 2 km, a thick layer of polluted air (2.5 to 5 km), an intrusion of convection from the boundary layer (6 to 7.5 km), and another layer of polluted air from 7.8 to 8.5 km. The highest polluted layer may have been part of the larger polluted air layer below it, then it may have been split from it by the air rising from the boundary layer through convection. The 500 hPa streamline map for 0000 UT on September 6 (not shown) suggests that the air sampled by the DC-8 at around 2145 UT may have moved southeast from 155°W, 15.5°S to 151°W, 17.5°S, where the P3-B intercepted it around 0300 UT. The distance between the two points was approximately 500 km, and the wind speed measured by the DC-8 and P3-B while in contact with the air mass was about 15 m/s. This wind speed only allows the air mass to travel about 250 km, but a greater speed at some point in the trajectory could have allowed the air to travel farther. The lidar images from the DC-8 suggest that the polluted (elevated ozone) layer had a large horizontal extent, increasing its chance of a reencounter with the P3-B. According to the lidar image the layer extended from at least 17.4°S, 153°W to 18°S, 155°W (Plate 4). The lidar also detected the thin polluted layer found by in situ instruments between 7.8 and 8.5 km. Again, the potential vorticity profile (Plate 5) shows elevated PV in the region where the DC-8 detected the high ozone layer, suggesting another large stratospheric intrusion.
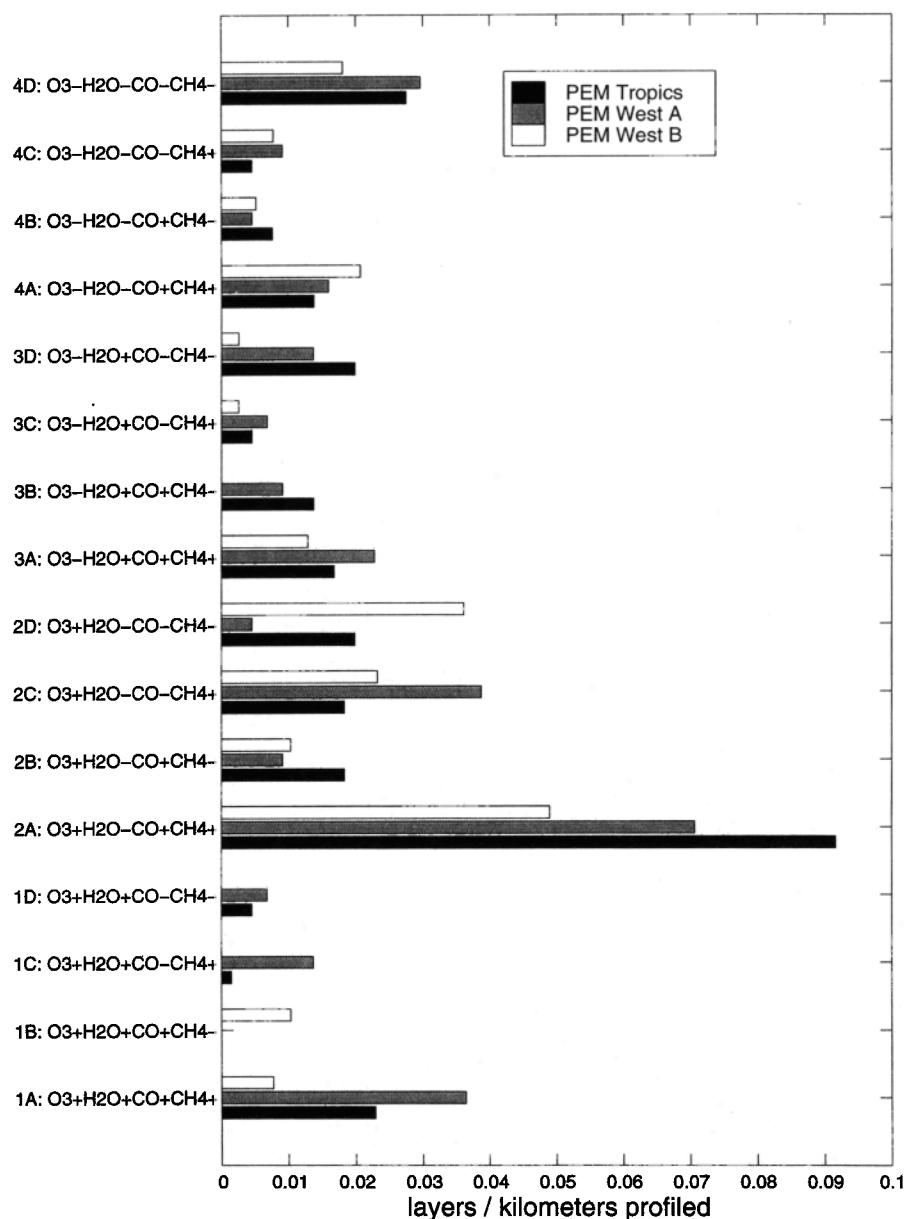
Figure 3. Number of layers detected per kilometer profiled. Layers are defined by O_3, H_2O, CO, and CH_4 deviations.

The P3-B flights off the South American coast were notable for the highly polluted air they encountered. Flight 17, for instance, encountered a layer of polluted air stretching from about 2.5 km to at least 4 km near 90°W, 3°S around 1600 UT. The peak CO mixing ratio was more than 300 ppbv in the layer, and the CH_4 mixing ratio was close to 1770 ppbv (Figure 7). Directly below, near 2 km, was another layer high in ozone, carbon monoxide, and methane.

6. Layer Influence on Atmospheric Temperature

The presence of layers with ozone and water vapor mixing ratios significantly different from the background atmosphere introduces changes in the radiative heating and cooling rates, which are strongly dependent on these gases. We show an example based on a typical ozonesonde profile taken at Tahiti during PEM-Tropics A (Figure 8). It was necessary to use ozonesonde data, as a complete vertical specification of temperature, ozone, and water vapor is needed in the radiative transfer program used [Hoffman, 1981]. The profile selected for September 18, 1996, includes a strong ozone layer in the 4-7 km region accompanied by very low water vapor. Above about 10 km, climatological values were used. The profiles of O_3 and H_2O were smoothed for water vapor, as shown in Figure 9, to simulate "no layer" conditions. The largest effect comes from the water vapor component of the layer, as shown in Figure 9: near 4 km the radiative cooling rate increases from about 1°C/d to 2.5°C/d, while near 6 km, it reduces from 1.5°C/d to close to zero. The net effect of relative cooling near the layer base and relative heating near the top is to stabilize the air in the layer and prevent vertical mixing across the layer. This self-stabilization may be an important factor in permitting extensive layers in the PEM-Tropics A region to
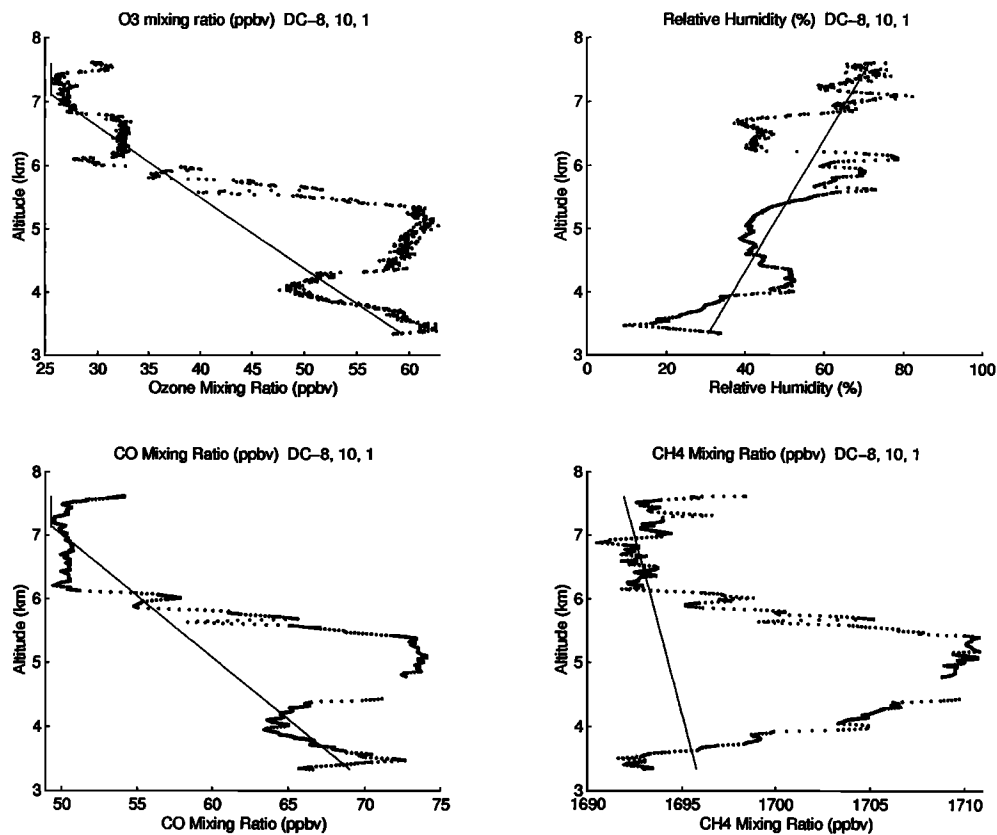
Figure 4. Vertical profiles of O_3, CO, CH_4, H_2O, and CO_2, sampled during PEM-Tropics A DC-8 mission 10 (September 14, 1996) around 2305 UT, near 144.6°W, 18.4°S. Thin lines are background levels as estimated by the new mode-based method.
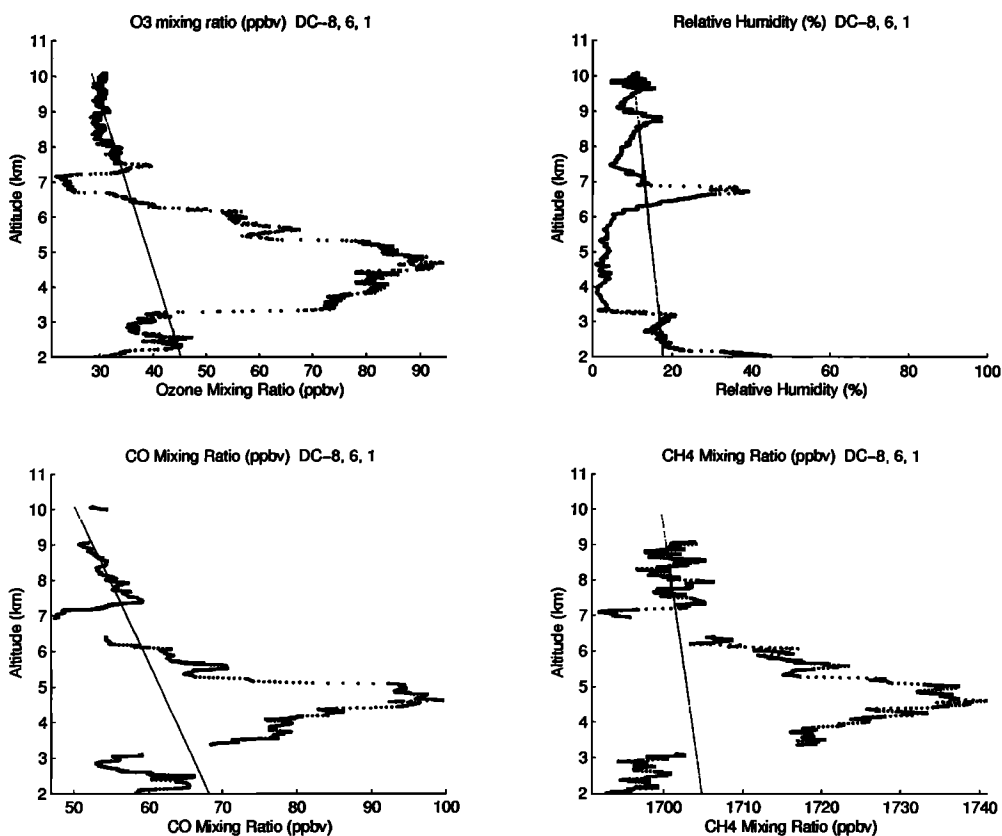

Figure 5. Vertical profiles of O_3, CO, CH_4, and H_2O, sampled during PEM-Tropics A DC-8 mission 6 (September 5, 1996) around 2145 UT, near 155°W, and 15.5°S. Thin lines are background levels as estimated by the new mode-based method.

CROSS−SECTION OF LIDAR O₃
PEM−TROPICS DC8 MISSION 10, STARTING ON 09/14/96
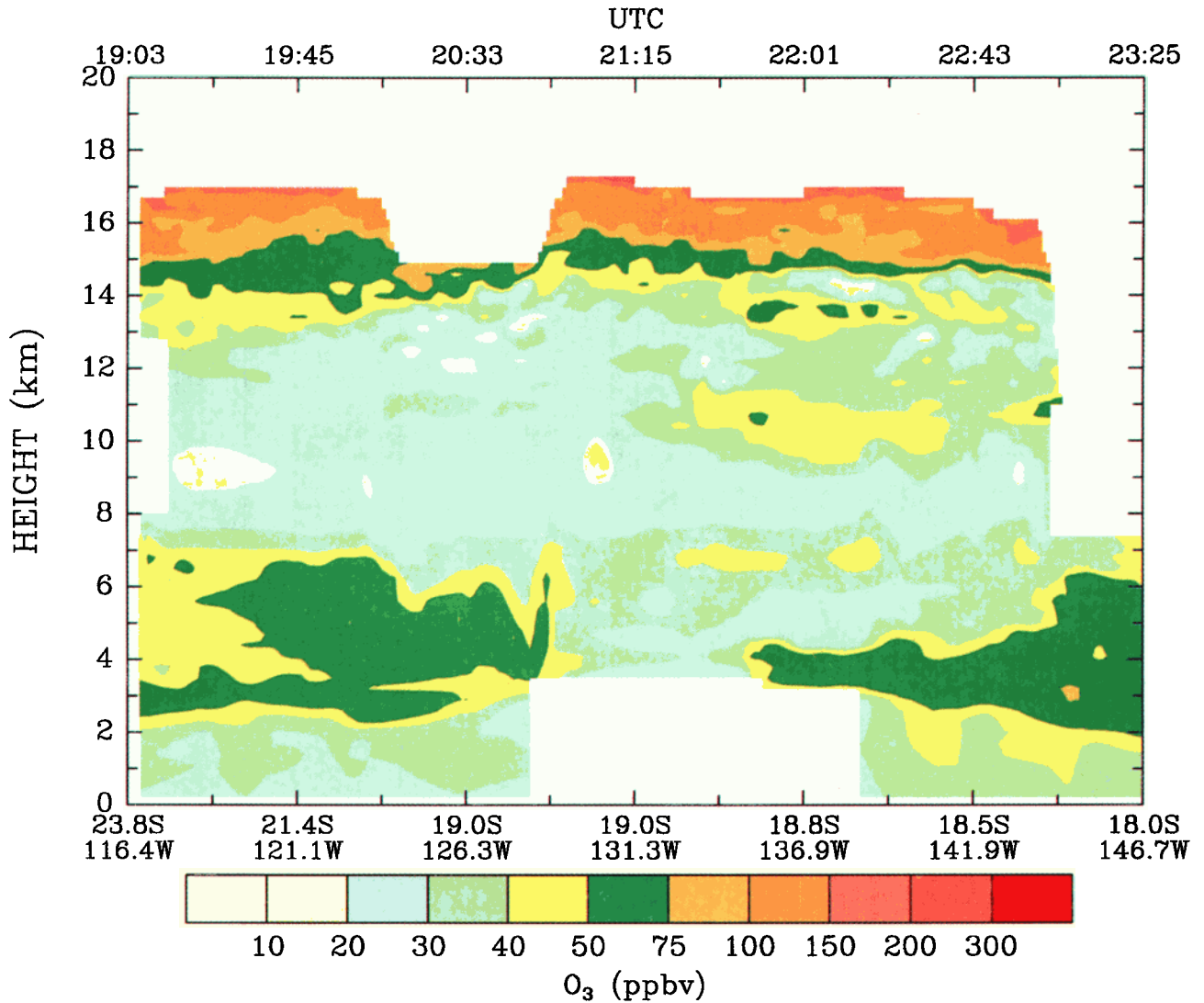
Plate 2. Cross sections of lidar O_3, PEM-Tropics A DC-8 mission 10, starting on September 14, 1996.

Plate 3. Cross sections of potential vorticity and potential temperature (K) from ECMWF data, starting on September 14, 1996.

CROSS–SECTION OF LIDAR O_3
PEM–TROPICS DC8 MISSION 06, STARTING ON 09/05/96
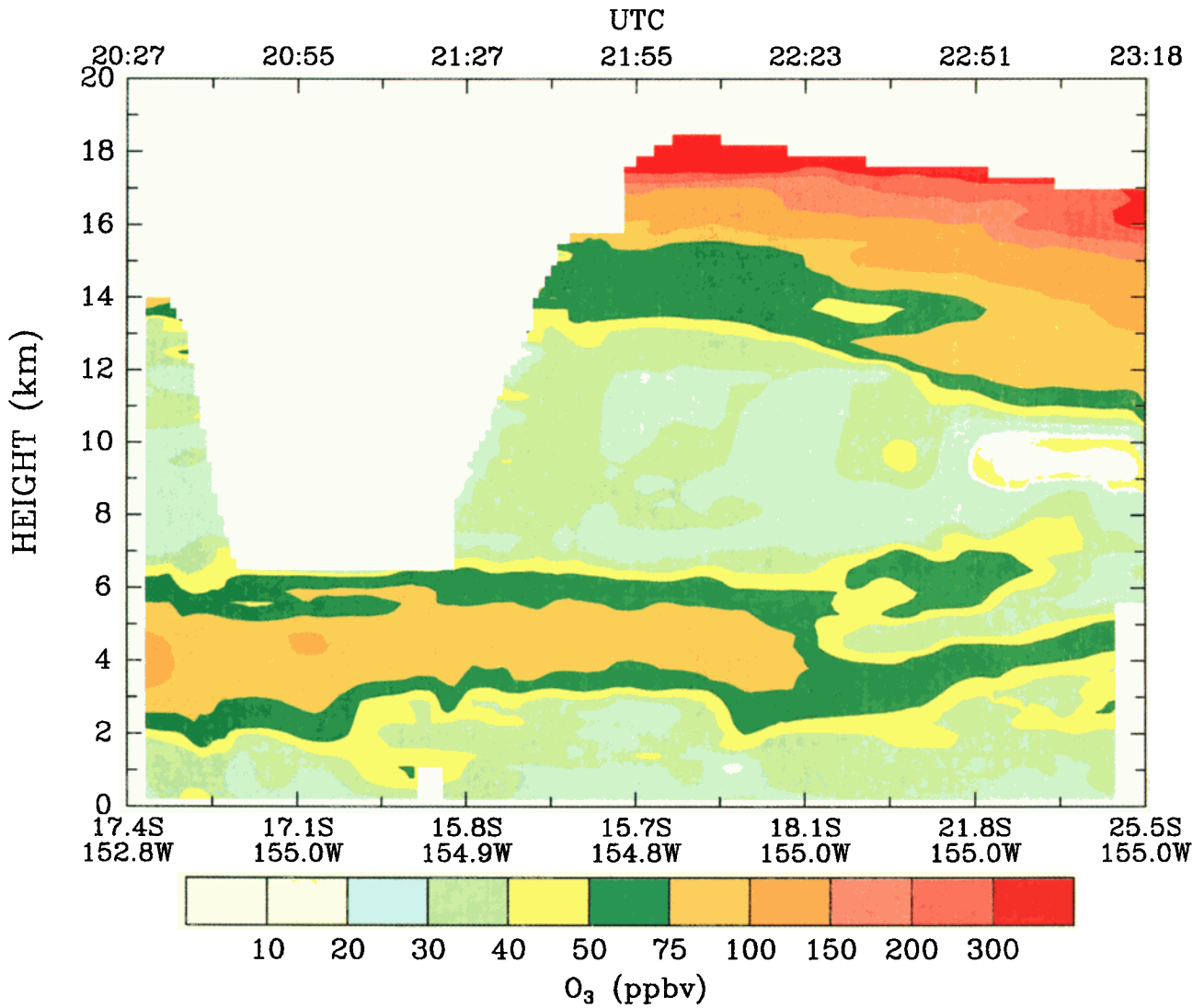
Plate 4. Cross sections of lidar O_3, PEM-Tropics A DC-8 mission 6, starting on September 5, 1996.

CROSS−SECTION OF POTENTIAL VORTICITY & POTENTIAL TEMPERATURE (K) ECMWF DATA, STARTING ON 09/05/96
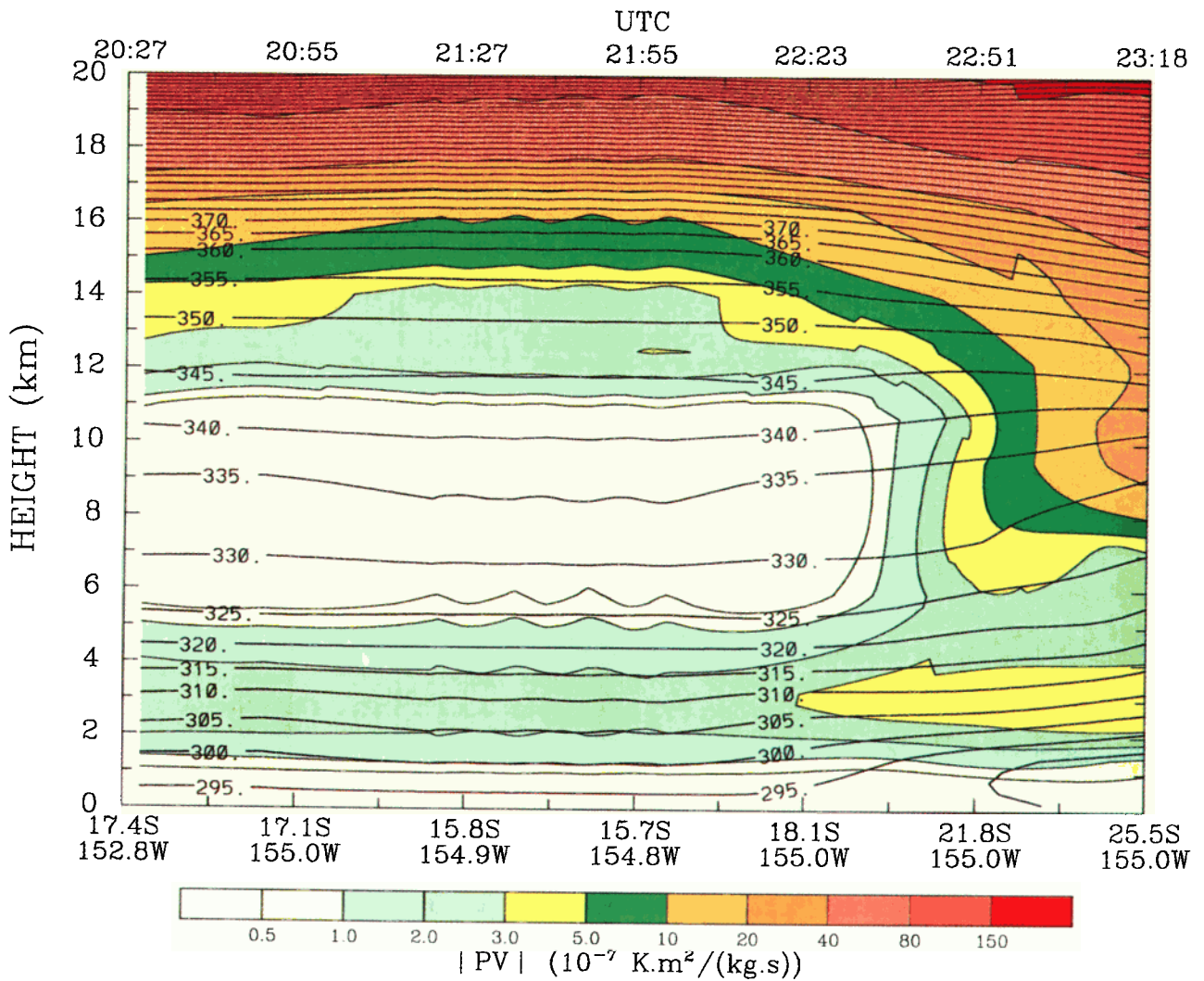
Plate 5. Cross sections of potential vorticity and potential temperature (K) from ECMWF data, starting on September 5, 1996.
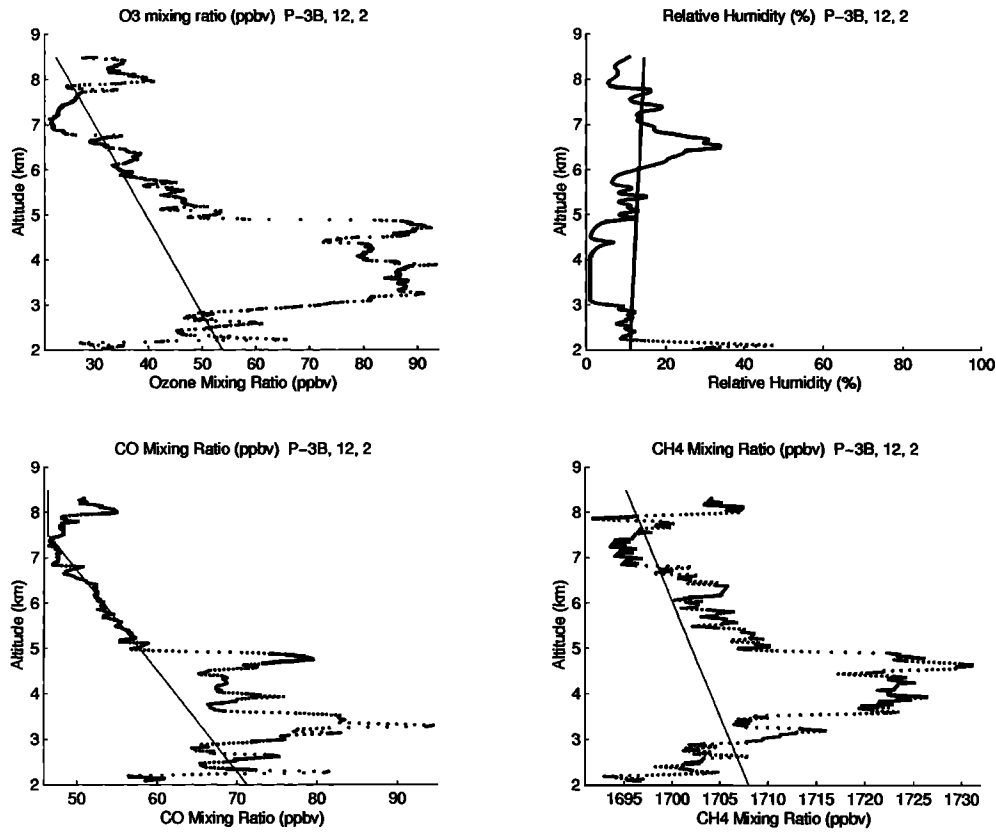
Figure 6. Vertical profiles of O_3, CO, CH_4, and H_2O, sampled during PEM-Tropics A P-3B mission 12 (September 5, 1996) around 0300 UT, near 151°W, 17.5°S. Thin lines are background levels as estimated by the new mode-based method.
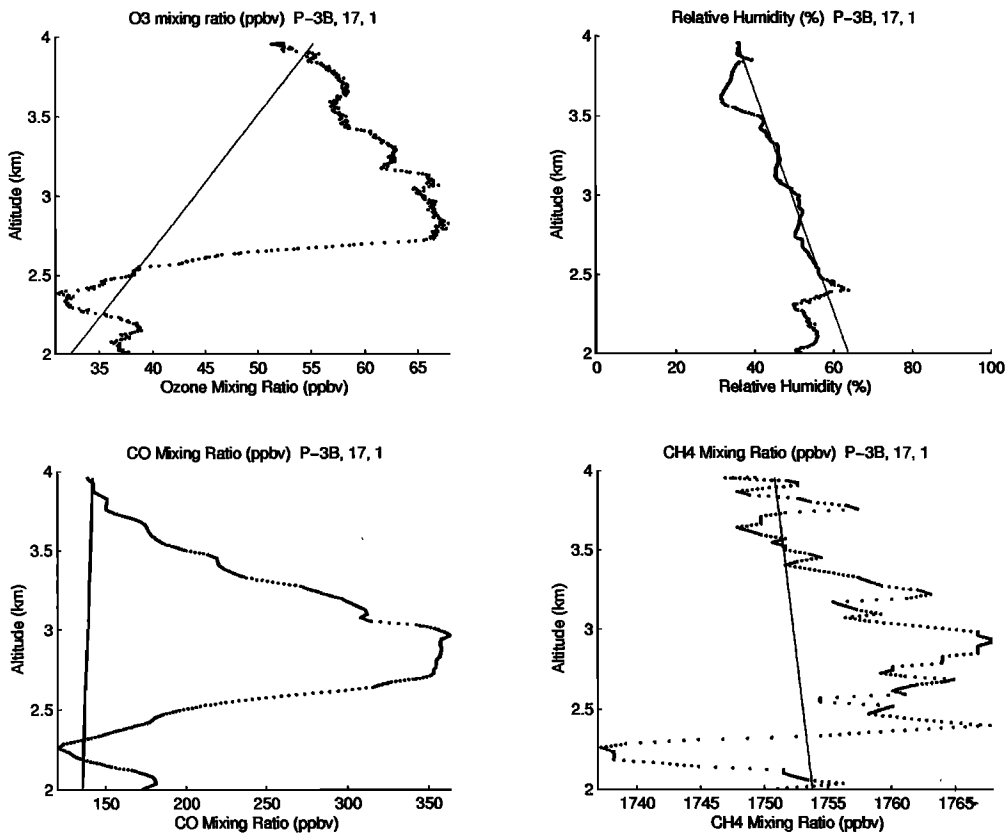
Figure 7. Vertical profiles of O_3, CO, CH_4, H_2O, and CO_2, sampled during PEM-Tropics A P-3B mission 17 around 1610 UT, near 90°W, 3°S. Thin lines are background levels as estimated by the new mode-based method.
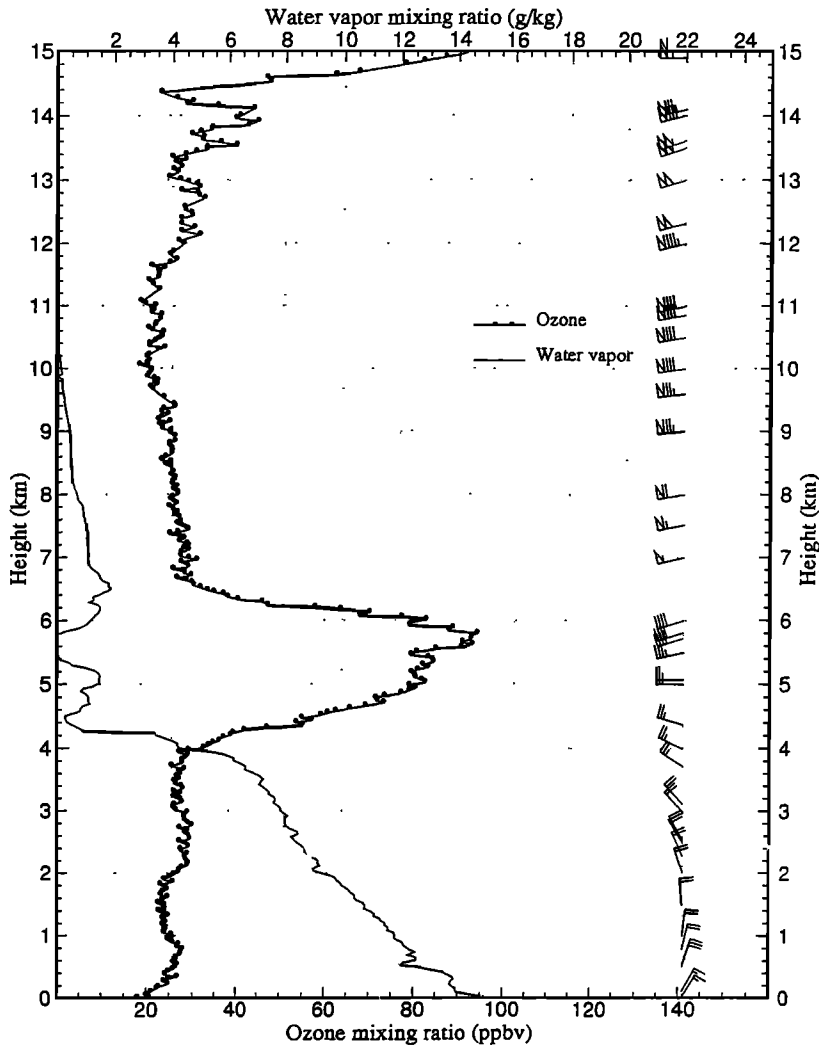
Figure 8. Ozonesonde data taken at Tahiti on September 18, 1996.

exist for relatively long periods. Eventually, large-scale sinking motion in the anticyclonic regions will move the air down into the boundary layer, where it will be mixed and oxidized, and the layer will lose its identity. The stabilization by radiative processes also will influence potential vorticity and complicate its use as a stratospheric tracer.

7. Conclusion

Of the layer production mechanisms summarized earlier, the most important is clearly the intrusion of stratospheric air into the troposphere. Not only does this produce layers of $+O_3$ - H_2O -CO -CH_4 air, but the strong stability of stratospheric air results in $+O_3$ -H_2O +CO +CH_4 layers by trapping otherwise buoyant plumes of pollution. However, especially over the tropics, convection penetrates to very high levels, and layers formed through stabilized convective plumes would tend to stretch to altitudes above the limit of the aircraft used. Thus our analysis probably underestimates such layers.

Clearly, by looking only at layers with ozone mixing ratio deviations from the background, we may be neglecting several types of layers. However, we should detect layers produced

by all of the mechanisms listed in Table 1. Clean marine air brought up from the boundary layer has a low ozone mixing ratio, compared to the free troposphere. Subsiding marine air originally brought up from the boundary layer should still have a low ozone mixing ratio; if it does not, then such layers have been effectively mixed into the free troposphere or are too large to be considered small-scale structure (defined as a few hundred meters thick for our purposes). Polluted air raised by convection should have elevated O_3, CO, and CH_4, as well as having a higher relative humidity than the background. Thus our results, though dealing with a limited layer sample, clearly suggest that stratospheric air mixed with pollution is the dominant source for ozone layers in the troposphere. Further studies with larger samples will be required to answer questions such as (1) How many polluted layers are formed without the help of stratospheric caps? (2) What are the geographical sources of these layers? The latter question is especially important for the relatively unexplored PEM-Tropics A sampling region.

This paper is the third in a series dealing with aircraft-detected layers. In the first two we used a 2-km sliding filter. Because of systematic overestimation of layer count with this approach, we incorporated a new mode-based method in this
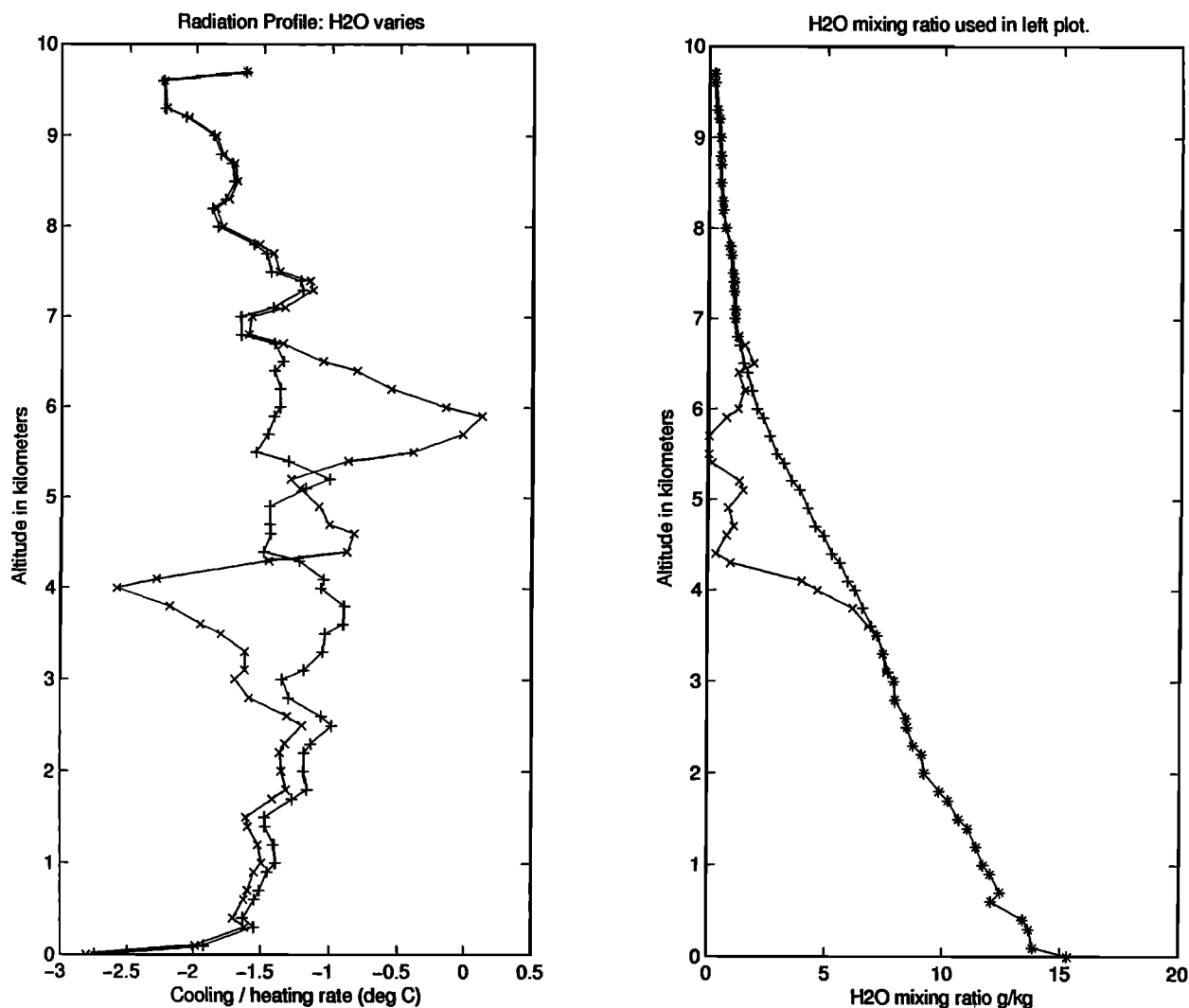
Figure 9. Radiative cooling rates for no-layer case (plusses) and layer case (crosses) using ozone and water vapor data from Figure 8.

paper and used it for PEM-Tropics A data as well as for the previous PEM-West data. As is evident from Figures 4, 5, and 6, the new method performs much better.

We have commenced a study of layers from ozonesondes and from aircraft lidar images to broaden the coverage. As noted previously, we think layers are frequent enough to be included in numerical and dynamical models involving chemical processes. In view of the nonlinearities involved, models of the type used by *Davis et al.* [1996] may be significantly altered by their inclusion.

References

Boldi, R. A., A model of the ion chemistry of electrified convection, Ph.D. thesis, Mass. Inst. of Technol., Cambridge, 206 pp., 1992.

Collins, J. E., Jr., B. E. Anderson, G. W. Sachse, J. D. W. Barrick, L. O. Wade, L. G. Burney, and G. F. Hill, Atmospheric fine structure during GTE TRACE A: Relationships among ozone, carbon monoxide, and water vapor, *J. Geophys. Res.*, *101*, 24,307-24,316, 1996a.

Collins, J. E., Jr., et al., Airborne nitrous oxide observations over the western Pacific Ocean: September-October 1991, *J. Geophys. Res.*, *101*, 1975-1984, 1996b.

Davis, D. D., et al., Assessment of ozone photochemistry in the western North Pacific as inferred from PEM-West A observations during the fall 1991, *J. Geophys. Res.*, *101*, 2111-2134, 1996.

Gregory, G. L., C. H. Hudgins, J. Ritter, and M. Lawrence, In situ ozone instrumentation for 10-Hz measurements: Development and evaluation, paper presented at the Sixth Symposium on Meteorological Observations and Instrumentation, Am. Meteorol. Soc., New Orleans, La., Jan. 12-16, 1987.

Hoell, J. M., et al., Pacific Exploratory Mission-West (PEM-West A): September-October 1991, *J. Geophys. Res.*, *101*, 1641-1653, 1996.

Hoell, J. M., D. D. Davis, S. C. Liu, R. E. Newell, H. Akimoto, R. J. McNeal, and R. J. Bendura, The Pacific Exploratory Mission-West Phase B: February-March, 1994, *J. Geophys. Res.*, *102*, 28,223-28,239, 1997.

Hoffman, R.N., A computer program which calculates radiative fluxes and heating rates in model atmospheres, *Sci. Rep. 4*, 124 pp., Dep. of Meteorol. and Phys. Oceanogr., Mass. Inst. of Technol., Cambridge, May 1981.

Intergovernmental Panel on Climate Change (IPCC), Trace gases and atmospheric chemistry, in *Climate Change, 1994*, edited by J. T. Houghton et al., pp. 85-87, Cambridge Univ. Press, New York, 1995.

Newell, R. E., Z.-X. Wu, Y. Zhu, W. Hu, E. V. Browell, G. L. Gregory, G. W. Sachse, J. E. Collins Jr., K. K. Kelly, and S. C. Liu, Vertical

fine-scale atmospheric structure measured from NASA DC-8 during PEM-West A, *J. Geophys. Res.*, *101*, 1943-1960, 1996.

Sachse, G. W., G. F. Hill, L. O. Wade, and M. G. Perry, Fast-response, high-precision carbon monoxide sensor using a tunable diode laser absorption technique, *J. Geophys. Res.*, *92*, 2071-2081, 1987.

Wu, Z.-X., R. E . Newell, Y. Zhu, B. E. Anderson, E. V. Browell, G. L. Gregory, G. W. Sachse, and J. E. Collins Jr., Atmospheric layers measured from the NASA DC-8 during PEM-West B and comparison with PEM-West A, *J. Geophys. Res.*, *102*, 28,353-28,365, 1997.

G.M. Albercook and M. A. Carroll, Department of Atmospheric, Oceanic, and Space Sciences, University of Michigan, 2455 Hayward, Ann Arbor, MI 48109-2143. (e-mail: mcarroll@umich.edu; galber@umich.edu)

B. E. Anderson, J. D. W. Barrick, E. V. Browell, G. L. Gregory, G. W. Sachse, and S. Vay, NASA Langley Research Center, 21 Langley Blvd., Hampton, VA 23681-0001. (e-mail: b.e.anderson@larc.nasa.gov; j.d.barrick@larc.nasa.gov; e.v.browell@larc.nasa.gov; g.l.gregory@larc.nasa.gov; g.w.sachse@larc.nasa.gov; s.a.vay@larc.nasa.gov)

J. Y. N. Cho, R. E. Newell, P. Stoller, V. Thouret, and Y. Zhu, Department of Earth, Atmospheric, and Planetary Sciences, Massachusetts Institute of Technology, 77 Massachusetts Ave., Rm. 54-1823, Cambridge, MA 02139-4307. (e-mail: jcho@pemtropics.mit.edu; newell@newell1.mit.edu; pstoller@pemtropics.mit.edu; valerie@newell3.mit.edu; zhu@newell1.mit.edu)

S. Sandholm, Baker Bldg., Rm. 107, School of Earth and Atmospheric Sciences, Georgia Institute of Technology, Atlanta, GA 30332. (e-mail: sts@minitower.gtri.gatech.edu)